[0.1, 1.1], where x is the physical coordinate normalized to wavelength, M_y is the y-component of the equivalent magnetic current, $H_0^{(2)}$ is the zero-order, second-kind Hankel function, η_0 is the intrinsic impedance in free space, and H_y^{inc} is the magnetic field intensity of the TE incident plane wave. Fig. 2 depicts the results of the magnitude of the equivalent magnetic current obtained using the periodic wavelet with $2^m = 128$ in comparison with the pulse function as the basis in moment method. The total number of periodic wavelet functions associated with the expansion with $2^m = 128$ is 256, as is also the total number of pulse functions used in the above computation. Good agreement can be observed between the two sets of results.

Unlike the case of the use of truncated wavelets on the real line in the moment method, where *strong* artificial oscillations almost definitely appear in the equivalent magnetic current magnitude near the boundary points no matter how high the resolution is selected in the wavelet expansion, the utilization of the periodic wavelets can suppress occurrences of oscillations near the boundary points as shown by Fig. 2. Due to the finite precision or resolution of computers and physical systems, solutions of problems under consideration are, in practice, represented in a finite resolution subspace. One major advantage of periodic wavelets is that, given a finite resolution 2^m, there always exists a set of periodic wavelet functions that forms a complete basis in the corresponding subspace $\mathbf{V}_m^{per} \subset L^2([0, 1])$. By setting a map between the finite interval under study and [0, 1], one can obtain a complete basis defined on the desired computation domain from the periodic wavelets. Quite the contrary, it is very difficult for a set of truncated wavelet functions on the whole real line to form a complete basis in a finite interval. The occurrence of oscillations in the equivalent magnetic current magnitude is a consequence for the lack of completeness in the basis near the boundaries.

As was expected for a wavelet expansion method, the use of periodic wavelets renders a sparse moment-method matrix. To examine the sparsity, a threshold procedure is imposed on the moment-method matrix. That is, in the moment-method matrix, the element is kept only if its magnitude relative to that of the largest one is above a selected threshold and set to zero otherwise. Fig. 3 illustrates the sparseness structures of the moment-method matrix obtained by using this technique with thresholds of 5×10^{-4} and 5×10^{-3}, where the black ink indicates the remaining nonzero elements. The ratio R of the number of the remaining nonzero elements to the total number of elements can be obtained as $R \approx 7.74\%$ and $R \approx 2.08\%$ for the respective thresholds selected above. Fig. 4 shows the magnitude of the equivalent magnetic current obtained by using the sparse matrices in Fig. 3. Note that with the threshold 5×10^{-4}, the number of the matrix elements drastically reduces to $R \approx 7.74\%$ after the threshold processing. Although only such a small ratio of matrix elements is employed, the resultant equivalent magnetic current is still quite accurate as shown by Fig. 4. When the threshold 5×10^{-3} is applied and the number of the used matrix elements further reduces to $R \approx 2.08\%$, some modest losses of accuracy appear near the boundaries in the resultant equivalent magnetic current as shown in Fig. 4. Considering that only a very small ratio (2.08%) of the matrix elements is used in this computation, the result is reasonably accurate.

IV. Conclusion

The utilization of periodic wavelet expansions in the moment methods has been proposed here. Comparing with their counterparts on the real line, the periodic wavelets are more suitable to handle the finite interval problems since they bypass the difficulties arising in the use of wavelets on the whole real line to expand the unknown functions defined over finite intervals. The periodic wavelet expansion preserves the capability of generating sparse moment-method matrix and adaptively fits itself to the various length scales. Numerical example shows that the periodic wavelet expansion gives better accuracy than the conventional wavelet expansion for finite interval problems.

References

[1] B. Z. Steinberg and Y. Leviatan, "On the use of wavelet expansions in the method of moments," *IEEE Trans. Antennas Propagat.*, vol. 41, pp. 610–619, May 1993.

[2] G. Wang and G. Pan, "Full wave analysis of microstrip floating line structures by wavelet expansion method," *IEEE Trans. Microwave Theory Tech.*, vol. 43, pp. 131–142, Jan. 1995.

[3] G. Wang, "Numerical techniques for electromagnetic modeling of high speed circuits," Ph.D. dissertation, Univ. of Wisconsin, Milwaukee, Oct. 1993.

[4] I. Daubechies, *Ten Lectures on Wavelet.* Philadelphia: SIAM Press, 1992.

[5] R. F. Harrington, *Field Computation by Moment Methods.* New York: IEEE Press, 1993.

Analytical Expressions for Simplifying the Design of Broadband Low Noise Microwave Transistor Amplifiers

Garry N. Link and V. S. Rao Gudimetla

***Abstract*—An analytical expression for the minimum achievable noise figure for a specified gain at a given frequency is derived for a microwave amplifier. The minimum noise figure is given in terms of the specified gain, the amplifier noise parameters, and the S parameters. Similarly, another expression for the maximum gain at a specified noise figure is derived in terms of the noise figure, the noise parameters, and the S parameters. It is shown that these expressions simplify the tradeoff considerations for broadband low noise amplifier design by avoiding the need to draw several constant noise and gain circles at each frequency of interest.**

I. Introduction

A broadband low noise amplifier is designed to meet a specified gain versus frequency profile, usually either flat gain or 6 dB/octave gain increase. The maximum acceptable noise figure over the entire bandwidth is also specified. To determine the minimum noise figure for the specified gain at a given frequency, the required gain circle is drawn on the Smith chart along with several noise figure circles [1], [2]. The minimum noise figure corresponds to the noise circle that is tangential to the gain circle. This process is repeated at each frequency of interest to ensure that the specified gain can be provided at or below the desired noise figure over the desired bandwidth. If not, a different device must be chosen or an additional tradeoff must

Manuscript received October 11, 1994; revised June 29, 1995.

G. N. Link was with Tektronix, Inc., MS 39-615, Beaverton, OR 97077-0001 USA. He is now with Maxim Integrated Products, Inc., Beaverton, OR 97005–1155 USA.

V. S. R. Gudimetla is with the Oregon Graduate Institute of Science and Technology, Department of EE/AP, Portland, OR 97291-1000 USA.

IEEE Log Number 9414239.

be made between the gain profile and the maximum allowed noise figure. In any case, this is a tedious design procedure.

The procedure outlined above would be greatly simplified if an analytical expression resulting in the minimum possible noise figure for a specified gain at a given frequency was available in terms of the specified gain and the published transistor parameters. Such an expression could be used to directly find the minimum noise figure for a specified gain at each frequency to determine if the specifications can be met. If the specifications cannot be met with the available devices, additional tradeoffs must be made between gain and noise specifications.

Alternatively, an analytical expression that provides the maximum possible gain in terms of the specified noise figure can be used with similar results.

In this paper, these equations are derived and used in an example to show the simplification possible in the design of broadband low noise amplifiers. In addition, expressions for the corresponding source reflection coefficients at each frequency are given.

Several related issues such as stability considerations [3], effects of feedback [4]–[6], and optimum terminations [7] in terms of the device noise parameters are discussed in detail in the literature, but the direct relationships between noise figure and gain have not been addressed.

In an important paper [8], Poole and Paul address a related problem which results in the optimization of the noise measure of an amplifier. The noise measure is a function of both the noise figure and the available gain. Such a result is important in some applications where a low noise amplifier is followed by a high gain amplifier. But, since the overall noise and S parameters of a cascaded two amplifier system can be calculated from the individual data for each amplifier, our technique is also applicable in this case. Also, unlike the results of Poole and Paul, the technique presented in this paper allows direct control of both the noise figure and the available gain. Therefore, our results are not precluded by the work of Poole and Paul.

II. Background

Equations (1)–(9) below are taken from [1] and [2]. The noise figure of a two port microwave amplifier at any frequency is given by

$$F = F_{\min} + \frac{4r_n|\Gamma_S - \Gamma_{opt}|^2}{(1-|\Gamma_S|^2)|1+\Gamma_{opt}|^2} \tag{1}$$

where $F_{\min}$, r_n, and Γ_{opt} are the published device noise parameters and Γ_S is the source reflection coefficient. The noise figure parameter is given by

$$\begin{aligned} N &= \frac{|\Gamma_S - \Gamma_{opt}|^2}{1-|\Gamma_S|^2} \\ &= \frac{F - F_{\min}}{4r_n}|1+\Gamma_{opt}|^2. \end{aligned} \tag{2}$$

On a Smith chart, the circular locus of all possible source reflection coefficient values that give a constant noise figure at a particular frequency can be drawn. The center (C_F) and radius (R_F) of this circle are given by

$$C_F = \frac{\Gamma_{opt}}{1+N} \tag{3}$$

$$R_F = \frac{1}{1+N}\sqrt{N^2 + N(1-|\Gamma_{opt}|^2)}. \tag{4}$$

Similarly, expressions exist for the center (C_a) and radius (R_a) of constant available gain (G_A) circles [9] which show the source reflection coefficient values that provide constant available gain at a given frequency. The symbol "*" in the equations below represents the complex conjugate operator

$$\begin{aligned} C_a &= \frac{g_a C_1^*}{1+g_a(|S_{11}|^2 - |\Delta|^2)} \\ &= L_1 C_1^* \end{aligned} \tag{5}$$

$$R_a = \frac{[1-2K|S_{12}S_{21}|g_a + |S_{12}S_{21}|^2 g_a^2]^{1/2}}{|1+g_a(|S_{11}|^2 - |\Delta|^2)|} \tag{6}$$

where

$$g_a = \frac{G_A}{|S_{21}|^2} \tag{7}$$

$$K = \frac{1-|S_{11}|^2 - |S_{22}|^2 + |\Delta|^2}{2|S_{12}S_{21}|} \tag{8}$$

$$C_1 = S_{11} - \Delta S_{22}^* \tag{9}$$

$$L_1 \equiv \frac{g_a}{1+g_a(|S_{11}|^2 - |\Delta|^2)}. \tag{10}$$

The constant L_1, which is related to the available gain, is defined to simplify the derivation of the new expressions.

Presently, iterative graphical techniques are used to find the value of source reflection coefficient that gives the minimum noise figure at a certain gain, or the maximum available gain at a given noise figure. After several constant noise figure and available gain circles are drawn on the same Smith chart, the source reflection coefficient can be extracted manually. Hence, analytical expressions are needed to directly provide the optimum source reflection coefficient to simplify the low noise microwave amplifier design process. These analytical expressions are presented below.

III. Maximum Available Gain for a Specified Noise Figure

At a given noise figure, the maximum gain occurs at the tangential intersection of the constant noise figure circle and the (unknown) optimum constant available gain circle. This can be represented analytically by

$$|C_a - C_F| = |R_a \pm R_F|. \tag{11}$$

It should be noted that two values of available gain will satisfy (11). These values correspond to the two possible gain circles that are tangential to the given noise figure circle. Care must be taken to ensure the optimum solution provides a source reflection coefficient that is passive and results in stable amplifier operation.

To derive the maximum available gain, R_a must first be given in terms of the transistor parameters and the available gain. Solving (10) for g_a and substituting the result into (6) gives

$$\begin{aligned} R_a = [1 + L_1^2\{&(|S_{11}|^2 - |\Delta|^2)(1-|S_{22}|^2) \\ &+ |S_{12}S_{21}|^2\} - L_1 B_1]^{1/2} \end{aligned} \tag{12}$$

where

$$B_1 = 1 + |S_{11}|^2 - |S_{22}|^2 - |\Delta|^2. \tag{13}$$

Using (9), (12) can be further simplified to

$$R_a = [1 + L_1^2|C_1|^2 - L_1 B_1]^{1/2}. \tag{14}$$

Substituting (5) and (14) into (11) and manipulating algebraically gives

$$\begin{aligned} &\pm 2R_F[1 + L_1^2|C_1|^2 - L_1 B_1]^{1/2} = \\ &\quad |C_F|^2 - 1 - R_F^2 \\ &\quad + L_1(B_1 - C_F C_1 - C_F^* C_1^*). \end{aligned} \tag{15}$$

Squaring (15) and rearranging results in the following quadratic equation:

$$A_2 L_1^2 + A_1 L_1 + A_0 = 0 \tag{16}$$

TABLE I
EXAMPLE DEVICE S PARAMETERS, NOISE DATA, AND MAXIMUM STABLE GAIN

f	S11		S12		S21		S22		F min	Rn	Gamma opt		MSG
(GHz)	Mag.	Ang.	Mag.	Ang.	Mag.	Ang.	Mag.	Ang.	(dB)	(Ohm)	Mag.	Ang.	(dB)
2	0.99	-14°	0.018	81°	1.93	166°	0.76	-8°	0.59	40.5	0.78	8°	20.3
4	0.98	-27°	0.034	72°	1.89	152°	0.75	-17°	0.7	35	0.76	24°	17.5
6	0.95	-40°	0.049	63°	1.82	139°	0.73	-24°	0.82	32	0.73	40°	15.7
8	0.92	-52°	0.06	55°	1.73	126°	0.72	-32°	0.96	30	0.73	54°	14.6
10	0.89	-64°	0.068	48°	1.64	114°	0.71	-39°	1.13	30.5	0.7	67°	13.8
12	0.86	-74°	0.074	42°	1.55	103°	0.69	-46°	1.3	30	0.66	80°	13.2
14	0.83	-84°	0.077	37°	1.45	93°	0.68	-53°	1.48	23	0.62	91°	12.8
16	0.8	-94°	0.077	33°	1.36	83°	0.67	-60°	1.68	16	0.59	104°	12.5
18	0.78	-103°	0.076	30°	1.28	73°	0.67	-66°	1.9	11.5	0.59	118°	9.99
20	0.76	-111°	0.074	29°	1.2	65°	0.66	-73°	2.13	8.5	0.58	127°	7.46
22	0.75	-119°	0.07	28°	1.13	56°	0.66	-79°	2.35	6.8	0.58	137°	6.18
24	0.74	-126°	0.066	30°	1.06	48°	0.66	-86°	2.56	5.7	0.59	145°	5.25
26	0.73	-133°	0.063	33°	1	41°	0.66	-92°	2.78	5	0.6	151°	4.54

where

$$A_2 = 4R_F^2|C_1|^2 - (C_F C_1 + C_F^* C_1^* - B_1^2) \tag{17}$$

$$A_1 = 2[(C_F C_1 + C_F^* C_1^*)(|C_F|^2 - 1 - R_F^2) + B_1(1 - |C_F|^2 - R_F^2)] \tag{18}$$

$$A_0 = -\frac{(1 - |\Gamma_{opt}|^2)^2}{(N+1)^2}. \tag{19}$$

The solution to this equation, obviously, is

$$L_1 = \frac{-A_1 \pm \sqrt{A_1^2 - 4A_0A_2}}{2A_2}. \tag{20}$$

This solution is a function of the S parameters, the noise parameters, and the specified noise figure. The optimum available gain values can now be calculated using (7), (10), and (20). The source reflection coefficient values are simply the point of intersection of the noise figure circle and the available gain circles. These intersections are represented mathematically by

$$\Gamma_S = C_F - \frac{C_a - C_F}{|C_a - C_F|} R_F \quad \text{for} \quad [|C_a - C_F| \le R_a \quad \text{and} \quad R_F \le R_a]$$

$$\Gamma_S = C_F + \frac{C_a - C_F}{|C_a - C_F|} R_F \quad \text{otherwise.} \tag{21}$$

The two solutions can be examined for stability.

IV. MINIMUM NOISE FIGURE FOR A SPECIFIED AVAILABLE GAIN

The minimum noise figure for a specified available gain is derived by first combining (3) and (4) to obtain the following result:

$$R_F^2 = \frac{N}{N+1} - N|C_F|^2. \tag{22}$$

Squaring (11) and substituting (22) gives

$$|C_F|^2(1+N) - C_F C_a^* - C_F^* C_a + |C_a|^2 - R_a^2 - \frac{N}{N+1} = 2R_a\sqrt{\frac{N}{N+1} - N|C_F|^2}. \tag{23}$$

Squaring (23), substituting (3), and rearranging terms results in a quadratic equation in terms of the noise figure parameter N

$$D_2N^2 + D_1N + D_0 = 0 \tag{24}$$

where

$$D_2 = (|C_a|^2 - R_a^2 - 1)^2 - 4R_a^2 \tag{25}$$

$$D_1 = 2(|C_a|^2 - R_a^2 - 1)(|\Gamma_{opt} - C_a|^2 - R_a^2) + 4R_a^2(|\Gamma_{opt}|^2 - 1) \tag{26}$$

$$D_0 = (|\Gamma_{opt} - C_a|^2 - R_a^2)^2. \tag{27}$$

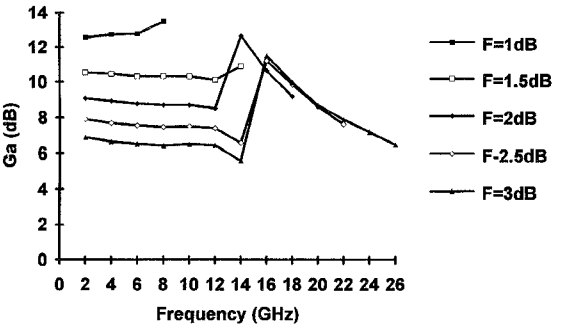

Fig. 1. Maximum available gain for several values of noise figure.

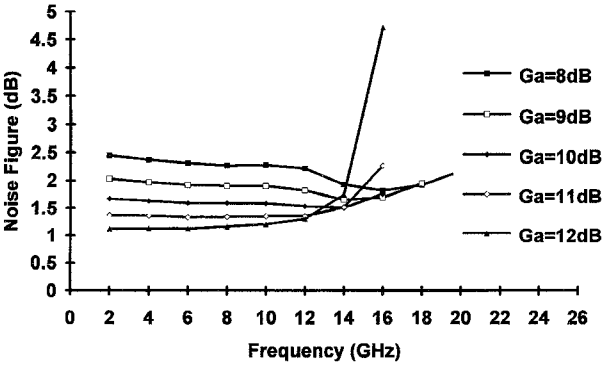

Fig. 2. Minimum noise figure for several values of available gain.

The solution to (24) is

$$N = \frac{-D_1 \pm \sqrt{D_1^2 - 4D_0D_2}}{2D_2}. \tag{28}$$

After choosing the minimum solution, (2) can be used to determine the optimum noise figure value in terms of the specified available gain and the amplifier parameters. Finally, (21) can be used to determine the source reflection coefficient.

V. EXAMPLE DESIGN

The Toshiba JS8830-AS microwave low noise GaAs FET has the S parameter and noise data given in Table I at a low noise bias point ($V_{DS} = 3$ V, $I_{DS} = 6$ mA).

Fig. 1 is a graph of the maximum available gain (subject to the maximum stable gain) that can be provided by this device for several values of noise figure as calculated using (20). This figure shows that this device is capable of providing a gain of more than 10 dB with a noise figure of 1.5 dB over a wide (2–14 GHZ) bandwidth. If it is desired to extend the bandwidth to 24 GHz with the same noise figure, the gain has to be reduced. The large change in maximum stable gain occurs where the optimum solution changes from the positive sign to the negative sign in (20). In other words, the optimum solution is changing from one side of the constant noise figure circle to the other.

Fig. 2 shows the minimum noise figure for several values of available gain. For example, if the required flat gain is 10 dB, the best possible noise figure is less than 2 dB from 2-16 GHz. The device is not capable of providing this amount of gain at higher frequencies.

VI. CONCLUSION

Analytical expressions have been developed to directly optimize the performance of microwave amplifiers. The expressions give the maximum available gain for a specified noise figure and the minimum noise figure for a specified available gain. The optimum source

reflection coefficient can then be calculated using the results of these expressions. These results can be extended to broadband microwave amplifier design by finding the optimum source reflection coefficient over a range of frequencies. The inclusion of these expressions in the advanced computer aided design tools that are now available would significantly simplify the low noise microwave amplifier design process.

REFERENCES

[1] G. D. Vendelin, A. M. Pavio, and U. L. Rohde, *Microwave Circuit Design Using Linear and Nonlinear Techniques.* New York: Wiley, 1990, pp. 84–93.

[2] G. Gonzalez, *Microwave Transistor Amplifiers: Analysis and Design.* Englewood Cliffs, NJ: Prentice-Hall, 1984, pp. 91–125.

[3] L. Besser, "Stability considerations of low-noise transistor amplifiers with simultaneous noise and power match," in *IEEE MTT-S Int. Microwave Symp. Dig.,* 1975, pp. 327–329.

[4] S. Iverson, "The effect of feedback on noise figure," *Proc. IEEE,* vol. 63, pp. 540–542, Mar. 1975.

[5] G. D. Vendelin, "Feedback effects on the noise performance of GaAs Mesfets," in *IEEE MTT-S Int. Microwave Symp. Dig.,* 1975, pp. 324–326.

[6] W. A. Suter, "Feedback and parasitic effects on noise," *Microwave J.,* pp. 123–129, Feb. 1983.

[7] H. Fukui, "Available power gain, noise figure, and noise measure of two-ports and their graphical representation," *IEEE Trans. Circuit Theory,* vol. CT-13, pp. 137–142, June 1966.

[8] C. R. Poole and D. K. Paul, "Optimum noise measure terminations for microwave transistor amplifiers," *IEEE Trans. Microwave Theory Tech.,* vol. MTT-33, no. 11, pp. 1254–1257, Nov. 1985.

[9] G. Gonzalez, *Microwave Transistor Amplifiers: Analysis and Design.* Englewood Cliffs, NJ: Prentice-Hall, 1984, pp. 92 and 123.

Simple and Explicit Formulas for the Design and Analysis of Asymmetrical V-Shaped Microshield Line

Kwok-Keung M. Cheng and Ian D. Robertson

Abstract— **This paper presents some simple, explicit and practical formulas for the evaluation of the quasi-TEM characteristic parameters of asymmetrical V-shaped microshield line, based on a conformal mapping procedure. These formulas give very accurate results in terms of elementary functions rather than the exact solution in terms of difficult functions. Two sets of expressions are described using first and second order approximations. These equations are easy to implement, thus making it an excellent choice for use in computer aided design, analysis and optimization of V-shaped microshield structures.**

I. INTRODUCTION

Recently, the microshield line, a new type of transmission line [1]–[4], has been the subject of growing interest as it has presented a solution to technical and technological problems encountered in the design of microstrip and coplanar lines. The microshield line, when compared with the conventional ones, has the ability to operate without the need for via-holes or the use of air-bridges for ground equalization. There are further advantages like reduced radiation loss, reduced electromagnetic coupling between adjacent lines, and the availability of a wide range of impedances. Various types of microshield structures have been reported [1], [2], and [4] including the rectangular, V, elliptic, and circular-shaped transmission lines. The quasi-TEM study of V-shaped microshield line (VSML) has been performed both by a method of moments [3] and a conformal mapping technique [4]. These methods give highly accurate results but are computationally intensive.

In this paper, a set of CAD-orientated closed form expressions that can be readily evaluated is derived for the characterisation of asymmetrical VSML. Both a first and a second order model for the approximation of the exact solution are presented. The analyses are based on the conformal mapping method and the assumptions of pure-TEM propagation and no dispersion effect. The characterization of the asymmetrical version of the VSML is extremely important because it could offer additional flexibility in the design of integrated circuits. Futhermore, it also allows one to evaluate the actual characteristics of a VSML normally designed to be symmetrical, but the fabrication of which is imperfect.

II. ANALYSIS OF ASYMMETRICAL VSML

This section gives a brief derivation of the characteristic parameters of an asymmetrical V-shaped microshield line. Similar mapping procedure has been described in [4] for a symmetrical line structure. The asymmetrical VSML configuration to be analyzed is shown in Fig. 1(a), where the ground plane is bent within the dielectric in a V-shape to form the equal sides of an isosceles triangle. All metallic conductors are assumed to be infinitely thin and perfectly conducting, and the ground planes to be sufficiently wide as to be considered infinite in the model. It is assumed that the air-dielectric boundary between the center conductor and the upper ground plane behaves like a perfect magnetic wall. This ensures that no electric field lines emanating into the air from the center conductor cross the air-dielectric boundary. Although this assumption is hardly verified for large slots, it has proven to yield excellent results for practical line dimensions. The center conductor, of width b, is placed between the two ground planes, which are located on a substrate of relative permittivity ε_r. The overall capacitance per unit length of the line can therefore be considered as the sum of the capacitance of the upper region (air) and the lower region (dielectric). The capacitance of the lower region can be evaluated through a suitable sequence of conformal mappings. First, the interior of the V-shaped region is mapped onto the t domain (Fig. 1) by the Schwartz-Christoffel transformation

$$z = A\int_0^t (t^2-1)^{(-2\beta+\pi)/2\pi}dt \tag{1}$$

and then back onto the w domain using a second mapping function

$$w = \int_0^t \frac{dt}{\sqrt{(t+t_E)(t-t_E)(t-t_C)(t-t_D)}} \tag{2}$$

where 2β is the flare angle (in radian) of the V-shaped wall. The intermediate parameters t_C, t_D and t_E, are evaluated by the following implicit expressions, as a function of β and the geometrical ratios, $d_1/b, d_2/b$ and b/W, of the structure

$$\frac{z_E}{z_B} = \frac{d_2+d_1+b}{W} = \frac{\zeta(\arcsin(t_E))}{\zeta(\pi/2)} \tag{3a}$$

Manuscript received November 29, 1994; revised June 29, 1995. This work was supported by The Engineering and Physical Sciences Research Council (EPSRC), UK.

The authors are with the Communication Research Group, Department of Electronic & Electrical Engineering, King's College London, University of London, Strand, London, England WC2R 2LS.

IEEE Log Number 9414243.